ACS Macro Letters

Letter

pubs.acs.org/macroletters

Near-Infrared Emitting Gold Cluster–Poly(acrylic acid) Hybrid Nanogels

Ying Chen,[†,‡,§] Xianchuang Zheng,[‡,§] Xin Wang,[‡] Chongzhi Wang,[‡] Yin Ding,[∥] and Xiqun Jiang*[,‡]

[†]Key Lab of Biomass Energy and Material, Institute of Chemical Industry of Forestry Products, CAF, Jiangsu Province, Nanjing, China

[‡]Department of Polymer Science and Engineering, College of Chemistry and Chemical Engineering, and Jiangsu Provincial Laboratory for Nanotechnology, Nanjing University, Nanjing, China

[∥]State Key Laboratory of Life Analytic Chemistry, Nanjing University, Nanjing, China

Supporting Information

ABSTRACT: A facile synthesis of near-infrared (NIR) luminescent gold cluster–poly(acrylic acid) (PAA) hybrid nanogels was developed by in situ reduction of gold salt in the core-hollow and shell-porous PAA nanogels. These Au-PAA nanogels exhibited excellent near-infrared photoluminescence properties and showed targeting potential in the optical imaging of the living body.

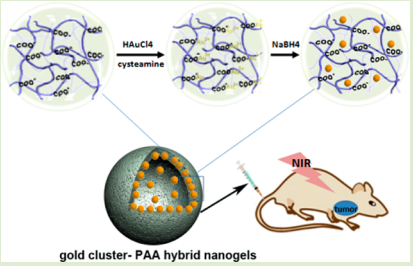

Gold nanoclusters (Au NCs) have gained considerable interest, arisen from their ultrasmall size (<2 nm) and size-dependent fluorescence properties.[1−4] So far, many efforts have been made in the synthesis of the Au NCs with florescence emission in the region of blue to near-IR (NIR).[5−7] An etching-based strategy was usually used to produce the Au NCs from large gold nanoparticles by etching with thiols,[8,9] biomolecules,[10] or multivalent polymers.[11] Recently biomimetic mineralization methods have been developed for facile preparation of the Au NCs using specialized polymers such as proteins,[12,13] dendrimers,[14] DNA,[15] and oligopeptides[16] as soft templates. The excellent fluorescent properties and low toxicity of the Au NCs make them a potential alternative to commonly used semiconductor quantum dots as labels for biosystem application.[17−19] However, up to present, the in vivo imaging of the Au NCs, especially NIR luminescent Au NCs, is still very limited. On the other hand, the polymer nanogels with the sizes of 50−200 nm hold the promise to be a highly efficient delivery platform for therapeutic agents and diagnostic probes due to good biocompatibility, high loading capacity, and effective targeting.[20−23]

In our previous work, poly(acrylic acid) (PAA) nanogels were prepared by the polymerization of acrylic acid monomer in the presence of hydroxypropyl cellulose (HPC) and cross-linking agent *N*,*N*-methylenebisacrylamide, followed by removal of HPC from the generated HPC-PAA nanoparticles.[24,25] These PAA nanogels had a hollow core and porous shell structure and showed particularly high drug loading capacity. As a significant advance in attempts to produce near IR emitting gold clusters, we present herein the synthesis of water-soluble gold cluster-encapsulated PAA hybrid nanogels (Au-PAA Ngs) and their bioimaging ability in the living body.

We used core-hollow and shell-porous PAA nanogels (Figure 1A) as soft templates, followed by in situ reduction of gold salt in aqueous solution, to prepare gold cluster-encapsulated PAA hybrid nanogels. The PAA matrix provides cavities for Au cluster nucleation and growth. Initially, PAA nanogels were mixed with cysteamine in aqueous solution. Owing to electrostatic interaction between COO^- groups of PAA and

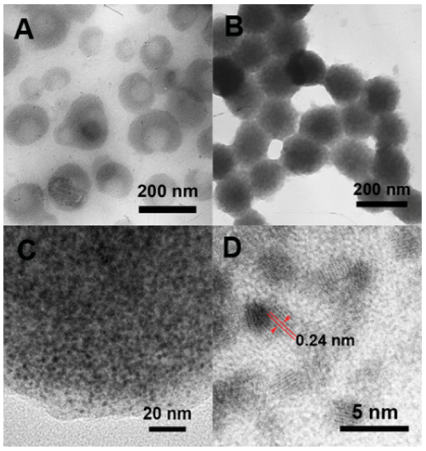

Figure 1. TEM images of (A) PAA nanogels; (B) Au-PAA Ngs and HRTEM (C, D) images of Au-PAA Ngs.

Received: November 8, 2013
Accepted: December 26, 2013
Published: December 30, 2013

NH_3^+ group of cysteamine, the cysteamine was sequestered into the PAA nanogels. Subsequently, $HAuCl_4$ solution was added slowly into the above PAA mixture solution, and Au(III) ions were reduced to Au(I) by thiols of cysteamine;[26] thus, Au(I) was entrapped into the cavities of PAA nanogels. Finally, the reduction agent, $NaBH_4$, was used to reduce Au(I) into gold clusters, and the color of the solution changed into light yellow (see Figure S1, SI), indicating the formation of the gold clusters.

The prepared Au clusters–PAA hybrid nanogels show typically spherical morphology and uniform size in the transmission electron microscope (TEM) image (Figure 1B). The average size of hybrid nanogels from TEM is about 150 nm, which is smaller than that measured by dynamic light scattering (DLS; see Figure S2, SI) due to nanogels' shrinking in the dry condition. The high resolution transmission electron microscope (HRTEM) images clearly demonstrate that a great number of ultrasmall gold clusters with the average diameter of about 1.7 nm are encapsulated in the PAA nanogels (Figure 1C,D), and their size distribution is narrow (see Figure S3, SI). The energy-dispersive X-ray (EDX) spectroscopy further confirms the presence of Au clusters in PAA nanogels (Figure S4, SI). Moreover, the well-resolved lattice planes of 0.24 nm spacing in the HRTEM image presents the crystalline structures of the resultant Au cluster (Figure 1D). The hybrid nanogels display excellent aqueous dispersibility, which is attributed to the large amount of carboxylic groups of PAA. It should be noted that changing the pH value of the reaction system to 8 before reduction was necessary in the process of preparation. Otherwise, only large Au nanoparticles (>20 nm) with irregular or plate-like morphologies were obtained, and these nanoparticles showed no luminescence. We think that the reduction ability of $NaBH_4$ is weakened at the medium pH of 8; hence, the entrapped gold ions endured progressive reduction to form gold clusters in the PAA nanogels cavities.

Next, the optical property of hybrid nanogels was investigated. Under near-infrared (NIR) light irradiation (λ_{ex} = 704 nm), the light yellow aqueous solution of Au-PAA Ngs emits an intense fluorescence (Figure 2 inset). In contrast, the control PAA nanogels solution shows no luminescence under the same treatment. The photoluminescence (PL) spectrum of the Au-PAA Ngs is presented in Figure 2, indicating that the hybrid nanogels possess a symmetrical PL peak with the maximum emission wavelength at 825 nm. This emission

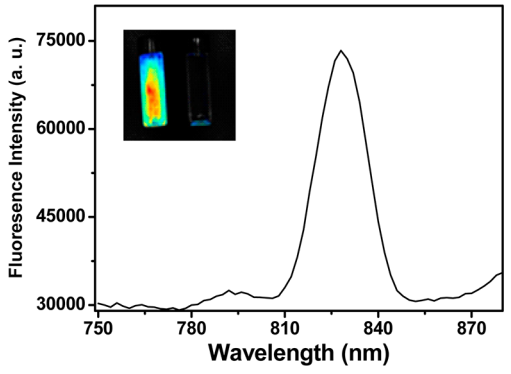

Figure 2. Photoemission (λ_{ex} = 704 nm) spectra of an aqueous solution of Au-PAA Ngs. The inset shows the photographs of Au-PAA Ngs (left) and PAA nanogels (right) aqueous solution under NIR light (λ_{ex} = 704 nm).

wavelength lies in the NIR emission range, which is a convenient window for in vivo imaging with deep penetration. The quantum yield of Au clusters in hybrid nanogels is determined to be 0.9% in the water (relative to 3,3′-diethyl-2,2′-thiatricarbocyanine iodide, 0.22% in ethanol). This is ~2-fold higher in magnitude than that of Au clusters synthesized with other routes.[27,28] Though this quantum yield of the Au clusters is still lower than that of most organic fluorophores and inorganic quantum dots, it is already in the range needed for applications in in vivo bioimaging. In particular, the excitation wavelength of the hybrid nanogels is in the NIR range, which can maximize tissue penetration and minimize optical absorption by physiologically abundant species such as hemoglobin.[29] Thus, it is reasonable to draw the conclusion that we have successfully synthesized luminescent Au clusters in PAA nanogels with both NIR emissions and excitation. The high stability of such hybrid nanogels in the aqueous system would greatly facilitate their use in in vivo applications.

To investigate the potential of NIR-emitting Au clusters in PAA nanogels for tumor imaging in living animals, the noninvasive and real-time NIR fluorescence imaging technique was performed. After the hybrid nanogels were subcutaneously injected into the left armpit of a healthy mouse, the mouse was imaged by fluorescence imaging system with 704 nm excitation and 745 nm emissions. Encouragingly, the bright fluorescence signal is clearly observed in the subcutaneous tissue of mouse under the NIR excitation (Figure. 3A). This suggests that the

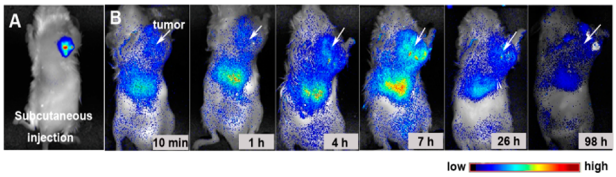

Figure 3. (A) In vivo image of the Au-PAA Ngs injected subcutaneously on left flank of a health mouse; (B) In vivo images of the Au-PAA Ngs in tumor-bearing mice.

emitting NIR fluorescence of Au clusters in PAA nanogels can be detected and imaged in the superficial area of the mouse. On the basis of this observation, we further examine the tumor imaging ability of the hybrid nanogels without any target group decoration after intravenous administration rather than subcutaneous injection into the mouse. After the hybrid nanogels with a concentration of 0.2 mg/mL were injected into subcutaneous hepatic H22 tumor-bearing mice via a tail vein (200 μL, per mouse), the mice were imaged at different time points (10 min, 1 h, 4 h, 7 h, 26 h, 98 h). The different fluorescence intensities are represented by different colors, as shown in the color histogram. Interestingly, the fluorescence signal in the tumor is already detected at 10 min postinjection (Figure 3B), although the strong fluorescence signal occurs at the liver region. With time escape, both signals from the tumor and liver regions become stronger and stronger. At 7 h postinjection, the tumor is well distinguished from surrounding tissues with good fluorescence contrast, implying high tumor uptake of the hybrid nanogels due to the enhanced permeability and retention (EPR) effect. After 7 h injection, the fluorescence intensity in tumor and liver tissues starts to decrease, although it can still be detected at 96 h postinjection, indicating that the hybrid nanogels accumulated in the organs are significantly cleared from the body within a period of 96 h.

dx.doi.org/10.1021/mz4005748 | ACS Macro Lett. 2014, 3, 74–76

In order to gain a deeper insight into the in vivo behavior of these Au-PAA Ngs and to prove that the fluorescence imaging indeed reflects the real accumulation of the hybrid nanogels in the organs, we analyzed the Au content in different organs using inductively coupled plasma (ICP) spectrometry. After intravenous administration of hybrid nanogels (0.2 mg/mL) into H22 tumor-bearing mice (200 μL, per mouse), we harvested and digested the different organs of the mice at 1, 6, 12, and 24 h postinjection for ICP analysis. The distribution profiles of Au in various tissues at different time points are displayed in Figure 4. It is found that the injected hybrid

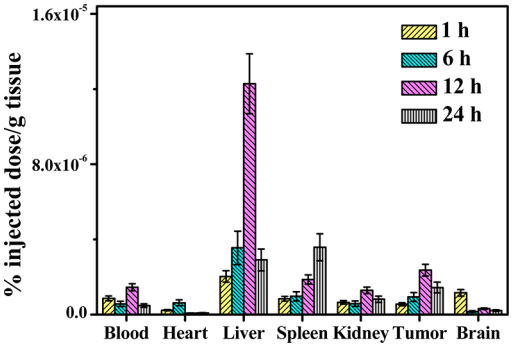

Figure 4. In vivo biodistribution of the Au-PAA Ngs over a period of 24 h in tumor-bearing mice.

nanogels mainly accumulate in the liver and spleen. The high Au concentration in the liver and spleen implies that probably the parts of the hybrid nanogels are inclined to be captured by the phagocytic cells of the reticuloendothelial system (RES) in the liver and spleen.[30−32] Meanwhile, the high tumor accumulation of Au is also observed. At 12 h postinjection, Au concentration in tumor tissue reaches its maximum and, after that, the Au concentration starts to decrease until the end of the test. Interestingly, we also find that the gold occurs at the brain region and reaches a maximum at 1 h postinjection. It seems that hybrid nanogels can cross the blood−brain barrier (BBB) and deliver gold to the brain. However, to address the delivery ability to the brain and demonstrate that the hybrid nanogels can cross the BBB, more experimental evidence is needed. Thus, the biodistribution profile of Au is in agreement with the NIR fluorescence observation.

In conclusion, we developed a facile synthesis of NIR luminescent Au-PAA Ngs by in situ reduction of gold salt in the core-hollow and shell-porous PAA nanogels. The Au-PAA Ngs possess strong photoluminescence, favorable biocompatibility, high drug loading capacity and excellent aqueous dispersibility. They are intrinsically suitable for bioimaging and therapeutic applications.

■ ASSOCIATED CONTENT

Ⓢ Supporting Information

Experimental details and additional results. This material is available free of charge via the Internet at http://pubs.acs.org.

■ AUTHOR INFORMATION

Corresponding Author

*E-mail: jiangx@nju.edu.cn.

Author Contributions

§These authors contributed equally (Y.C. and X.Z.).

Notes

The authors declare no competing financial interest.

■ ACKNOWLEDGMENTS

This work was supported by the National Natural Science Foundation of China (Grant No. 31100427, 21105047, 51033002 and 51273090), the Jiangsu Province Natural Science Foundation (BK20131071), and Program for Changjiang Scholars and Innovative Research Team in University.

■ REFERENCES

(1) Saha, K.; Agasti, S. S.; Kim, C.; Li, X.; Rotello, V. M. *Chem. Rev.* **2012**, *112*, 2739.
(2) Boisselier, E.; Astruc, D. *Chem. Soc. Rev.* **2009**, *38*, 1759.
(3) Llevot, A.; Astruc, D. *Chem. Soc. Rev.* **2012**, *41*, 242.
(4) Lopez-Acevedo, O.; Kacprzak, K. A.; Akola, J.; Häkkinen, H. *Nat. Chem.* **2010**, *2*, 329.
(5) Shang, L.; Azadfar, N.; Stockmar, F.; Send, W.; Trouillet, V.; Bruns, M.; Gerthsen, D.; Nienhaus, G. U. *Small* **2011**, *7*, 2614.
(6) Santiago González, B.; Rodríguez, M. a. J.; Blanco, C.; Rivas, J.; López-Quintela, M. A.; Martinho, J. M. G. *Nano Lett.* **2010**, *10*, 4217.
(7) Polavarapu, L.; Manna, M.; Xu, Q.-H. *Nanoscale* **2011**, *3*, 429.
(8) Jin, R. *Nanoscale* **2010**, *2*, 343.
(9) Negishi, Y.; Igarashi, K.; Munakata, K.; Ohgake, W.; Nobusada, K. *Chem. Commun.* **2012**, *48*, 660.
(10) Zhou, R.; Shi, M.; Chen, X.; Wang, M.; Chen, H. *Chem.—Eur. J.* **2009**, *15*, 4944.
(11) Duan, H.; Nie, S. *J. Am. Chem. Soc.* **2007**, *129*, 2412.
(12) Xie, J.; Zheng, Y.; Ying, J. Y. *J. Am. Chem. Soc.* **2009**, *131*, 888.
(13) Chaudhari, K.; Xavier, P. L.; Pradeep, T. *ACS Nano* **2011**, *5*, 8816.
(14) Boisselier, E.; Diallo, A. K.; Salmon, L.; Ornelas, C.; Ruiz, J.; Astruc, D. *J. Am. Chem. Soc.* **2010**, *132*, 2729.
(15) Li, T.; Zhang, L.; Ai, J.; Dong, S.; Wang, E. *ACS Nano* **2011**, *5*, 6334.
(16) Dickson, R. M.; Zheng, J. U.S. Patent 7,611,1907 B2, 2009.
(17) Sun, C.; Yang, H.; Yuan, Y.; Tian, X.; Wang, L.; Guo, Y.; Xu, L.; Lei, J.; Gao, N.; Anderson, G. J. *J. Am. Chem. Soc.* **2011**, *133*, 8617.
(18) Cheng, Y.; Meyers, J. D.; Broome, A.-M.; Kenney, M. E.; Basilion, J. P.; Burda, C. *J. Am. Chem. Soc.* **2011**, *133*, 2583.
(19) Chen, H.; Li, B.; Ren, X.; Li, S.; Ma, Y.; Cui, S.; Gu, Y. *Biomaterials* **2012**, *33*, 8461−8476.
(20) Soppimath, K. S.; Aminabhavi, T. M.; Kulkarni, A. R.; Rudzinski, W. E. *J. Controlled Release* **2001**, *70*, 1.
(21) Kataoka, K.; Harada, A.; Nagasaki, Y. *Adv. Drug Delivery Rev.* **2001**, *47*, 113.
(22) Chen, Y.; Wilbon, P. A.; Zhou, J.; Nagarkatti, M.; Wang, C.; Chu, F.; Tang, C. *Chem. Commun.* **2013**, *49*, 297.
(23) Oh, J. K.; Lee, D. I.; Park, J. M. *Prog. Polym. Sci.* **2009**, *34*, 1261.
(24) Chen, Y.; Zheng, X.; Qian, H.; Mao, Z.; Ding, D.; Jiang, X. *ACS Appl. Mater. Inter.* **2010**, *2*, 3532.
(25) Chen, Y.; Ding, D.; Mao, Z.; He, Y.; Hu, Y.; Wu, W.; Jiang, X. *Biomacromolecules* **2008**, *9*, 2609.
(26) Shon, Y.-S.; Gross, S. M.; Dawson, B.; Porter, M.; Murray, R. W. *Langmuir* **2000**, *16*, 6555.
(27) Lee, D.; Donkers, R. L.; Wang, G.; Harper, A. S.; Murray, R. W. *J. Am. Chem. Soc.* **2004**, *126*, 6193.
(28) Huang, T.; Murray, R. W. *J. Phys. Chem. B* **2001**, *105*, 12498.
(29) Hilderbrand, S. A.; Weissleder, R. *Curr. Opin. Chem. Biol.* **2010**, *14*, 71.
(30) Cho, K.; Wang, X.; Nie, S.; Shin, D. M. *Clin. Cancer Res.* **2008**, *14*, 1310.
(31) Wu, W.; Li, R.; Bian, X.; Zhu, Z.; Ding, D.; Li, X.; Jia, Z.; Jiang, X.; Hu, Y. *ACS Nano* **2009**, *3*, 2740.
(32) Ding, D.; Li, K.; Zhu, Z.; Pu, K.-Y.; Hu, Y.; Jiang, X.; Liu, B. *Nanoscale* **2011**, *3*, 1997.